MANUFACTURE AND SURFACE ANALYSIS OF THE Al-ALLOY VACUUM CHAMBER FOR SPring-8

S. Yokouchi, YoungPak Lee,* H. Sakamoto,**
T. Nishidono, Y. Morimoto, and Suck Hee Be
RIKEN-JAERI Synchrotron Radiation Facility Design Team
2-28-8 Honkomagome, Bunkyo-ku, Tokyo 113, Japan

Abstract

SPring-8 is in the progress of design as an 8 GeV high - brilliance synchrotron radiation source. We test-manufactured the Al-alloy vacuum chambers for the R&D of vacuum system of the main storage ring. The specifications were tested and evaluated. Moreover, we analyzed the treated surface by means of AES and SEM.

Introduction

The vacuum chambers for our main storage ring consist of two types, straight-section and bending-magnet chambers. The manufactured chambers are made of extruded Al alloy (A6063-T5), and 4 m long. Their cross sections are shown as in Fig. 1 (a) and (b). The extruded Al alloy is employed because of (1) the easy fabrication for complicated cross-sectional shapes, (2) low outgassing rate after baking at as low as 150°C, (3) rapid damping of residual radioactivity, (4) light weight, and finally (5) high thermal conductivity . The extruded material itself has undergone the mechanical and chemical composition analysis. We have also checked the dimensional accuracy, and surface roughness, especially across the direction of extrusion. The completed chambers were exposed to He-leak test and measurement of the displacement during evacuation, together with the evaluation of outgassing rate (q). All the results turn out to be valid with respect to the specifications. In addition, the outgassing-rate, which is very important to achieve ultra-high vacuum for the required beam lifetime, was measured to be as low as 10^{-13} Torr·l/sec·cm^2 after a baking at ~ 140°C for 40 hours. The outgassing rate, and desorption induced by high-energy photons and their photoelectrons are known to have correlation with the condition of surface. We have also analyzed the surface of chamber by Auger Electron Spectroscopy (AES) and Scanning Electron Microscopy (SEM) in mind for the gas loads. Furthermore, since some unexpected specks of extra corrosion were seen on one of our cleaned chambers, we also figure out the nature and origin at the same time.

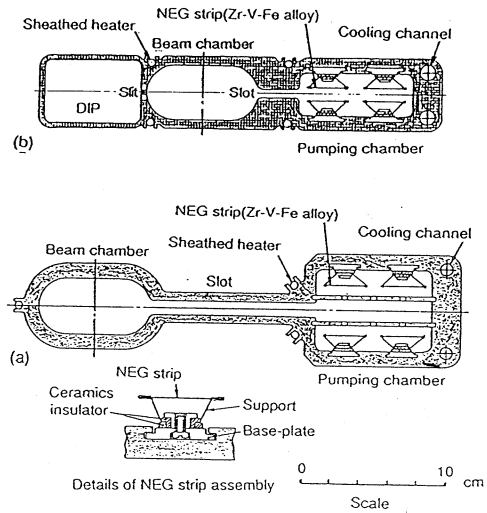

Fig. 1 The cross-sectional views of (a) straight-section and (b) bending-magnet chambers.

* On leave from RIST, Pohang, Korea.
** Ishikawajima-Harima Heavy Industries Co., Ltd.

Specifications The specifications can be summarized as below.

Materials and extrusion
(1) Extrusion under Ar + O_2 in the same way as for A6063-T5, but the mechanical characteristics should be equivalent to T6 (JIS H 4100).
(2) Chemical composition: JIS H 4100 except with Zn ≤ 0.01%.
(3) Dimensional accuracy: Special grade in JIS H 4100, but an axis distortion of ≤ 2.0 mm / 2000 mm.
(4) Surface roughness of inner surface: $R_{max} \leq 10$ μm.

Chambers
(1) Allowable quantity of leak: ≤ 1 x 10^{-10} Torr·l/sec·cm^2 on the He-leak detector.
(2) Strength to withstand an external stress of 1 kgf/cm^2.
(3) q ≤ 5 x 10^{-12} Torr·l/sec·cm^2 (determined by a pressure-profile calculation for the vacuum system of storage ring).

Procedure The manufacture process is represented in Fig. 2. The emphasis in each step is also pointed out.

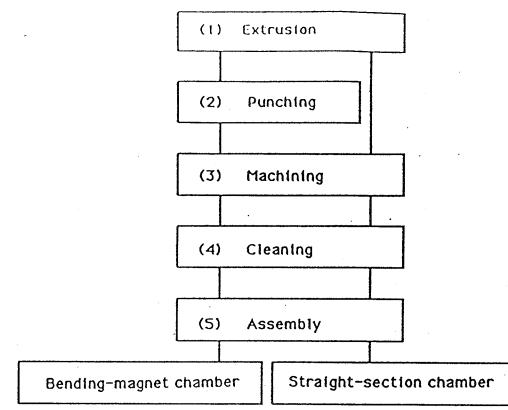

Fig. 2 The manufacture process for vacuum chambers.

Test and evaluation

The tensile strength and chemical composition of extruded material were checked according to JIS Z 2201 and 2241, and JIS H 1305, respectively, and the results are satisfied with the specifications. The dimensional accuracy turned also out to be valid. The surface roughness of inner surface was represented by R_{max} = 3.0 - 8.0 μm.

As for the completed chambers, first of all, He-leak test was performed at an allowable leak of 1 x 10^{-10} Torr·l/sec. No leak was observed. The displacement of straight-section chamber (SSC) during evacuation from atmosphere was also found (Table 1) to be its maximum of 1.05 mm at points 3 and 4. Fig. 3 shows a computer analysis of the deformation of SSC for the stress induced by evacuation from atmosphere by means of a general code for structure analysis, MSC/NASTRAN. The calculation revealed the maximum displacement of 0.894 mm. When we consider that the measured thicknesses at those points are a little thinner than the designed, we notice a fair agreement between the calculation and measurement suggesting that the stress is really within that for calculation.

unit mm

Measure point	(1)	(2)	(3)	(4)	(5)	(6)
Dial gauge indication	0.185	0.110	0.530	0.520	0.115	0.1
Measured displacement		0.295		1.05		0.225
Calculated displacement (=2δy)		——		0.894		——

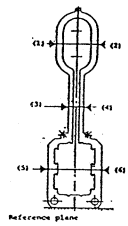

Table 1. The deformation during evacuation from atmosphere.

No.	Principal stress kgf/mm²	Principal shearing stress kgf/mm²	Allowable stress kgf/mm²
(1)	2.117	2.289	4.0
(2)	−2.602	2.511	
(3)	−2.466	2.400	
(4)	−1.900	1.872	

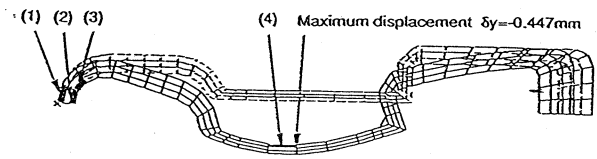

Fig. 3 A computer analysis of the deformation of straight-section chamber by means of MSC/NASTRAN.

q was obtained by throughput method making use of

$$q = C(p_1 - p_2)/A, \quad (1)$$

where C is the conductance of orifice (2.32 l/sec for N_2), p_1 and p_2 the pressures in Torr at IG 1 and 2, respectively, and A the total surface area of sample in cm^2. V 2 has been open for TMP 2 only when the chamber pressure was too high. The measuring system is given schematically in Fig. 4. Fig. 5 shows q vs. pumping time for SSC. We obtained q in the orders of 10^{-10} and 10^{-11} Torr·l/sec·cm^2 after ~ 100 and a few 100 hour evacuation, respectively, without baking. After a baking at ~ 140°C for 40 hours, q was measured to be even a low 10^{-13} Torr·l/sec·cm^2.

The q of bending-magnet chamber was also measured with non-evaporable getter (NEG) strips in it (Fig. 6). In this case, we have another source of q from the surface of NEG strips and their support (SUS 304 and ceramics) as well as the chamber itself. This contribution from the NEG strips will be, of course, gone after the activation. Since the separate evaluation of q from each material was very difficult, we got the overall q using Eq. (1) with the overall A. The q was ~ 10^{-10} Torr·l/sec·cm^2 after a pumping of a few 10 hours without baking, which turns out to be almost same as for SSC. On the other hand, the q was higher by an order to be low 10^{-12} - high 10^{-13} Torr·l/sec·cm^2 after baking at the same condition as for SSC. This can be interpreted by the fact that the bakeout was not enough for the NEG strips and their support. No problem is foreseen in the real storage ring where the NEG is working, because we were able to get the specifications only with a baking at ~ 140°C for 40 hours.

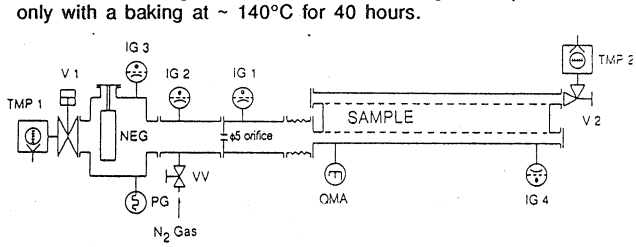

IG 1, 2, 3, 4 : Ionization gauge
NEG : Non-evaporable getter strip
V2 : Right angle valve
QMA : Quadrupole mass analyzer
TMP 1,2 : Turbo-molecular pump
V 1 : Pneumatically operated gate valve
VV : Venting valve
PG : Pirani gauge

Fig. 4 The schematic diagram of measurement setup for outgassing rate.

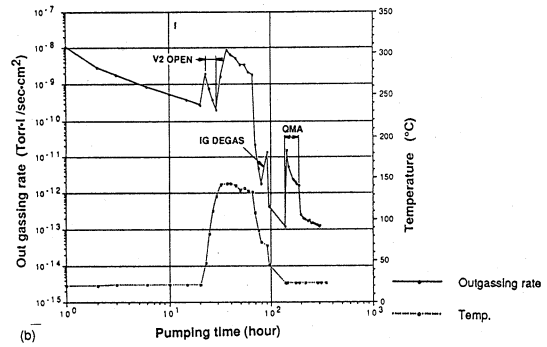

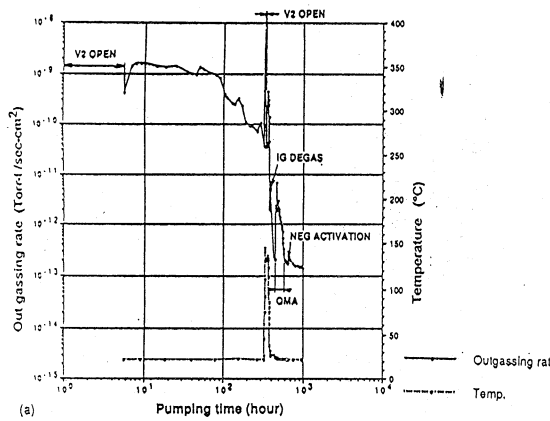

Fig. 5 q vs. pumping time of SSC without non-evaporable getter strips. A = 30000 cm^2. (a) the first measurement, and (b) after an exposure to N_2 of ~ 1 atm for 20 days.

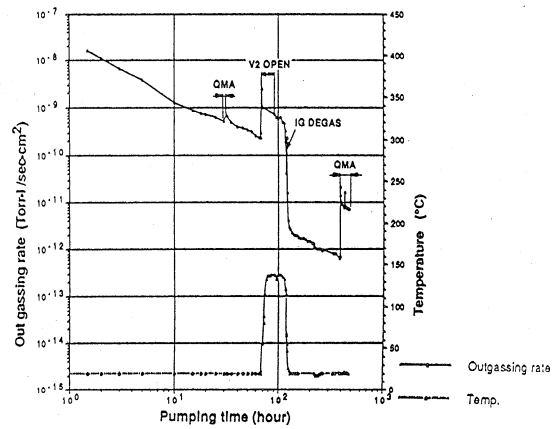

Fig. 6 q vs. pumping time of bending-magnet chamber with NEG strips. A = 56000 cm^2 (30700 cm^2 for the chamber itself, and 8700 and 16600 cm^2 for the NEG strips and their support, respectively).

Therefore, we are able to say that the chambers were submitted satisfactorily to the specifications as for the vacuum system of 8 GeV storage ring.

Surface analysis

Experimentals AES and SEM were carried out in JEOL JAMP 30 Auger Microprobe. For AES, E_p = 5 keV and i_e = 500 nA. When ion bombardment was required for depth profile, an ion sputter gun was used at V_{ion} = 3 keV, and i_{ion} = 30 nA with a homogeneous raster of 300 x 300 μm^2.

Results and discussion Three distinct samples were prepared from the chamber. Sample A and B represent the ordinary surface

before and after the cleaning process, respectively. On the other hand, Sample C was picked up to include the extraordinary corrosion specks. They didn't exist on the original extruded surface.

Sample A shows that the intensity (I) of Al KLL peak is only 0.333 times that of Mg KLL peak. This measured $I_{Al\ KLL} / I_{Mg\ KLL}$ is much smaller than the limit for bulk (89.941) suggesting a Mg oxide-rich layer for the top 30 Å as in Ref. 1. On Sample B, all the I's were decreased, suggesting a less dense oxide and contamination at the top. This may be attributed to the cleaning procedure. On the other hand, the top 30 Å shows more Mg oxide-rich than A to be $I_{Al\ KLL} / I_{Mg\ KLL} = 0.206$. Three characteristic points were investigated for Sample C. Point C-1 was picked up from the speck on the left in Fig. 7. Point C-2 is on the top smaller speck of the right side one, which looks another phase of corrosion-growth. The other probing point is on a heavily-oxidized particle of small size in the border itself for the left speck.

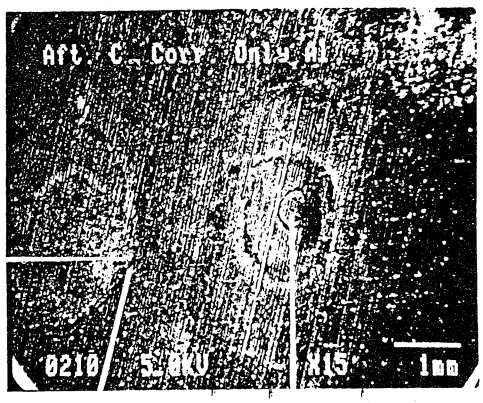

Fig. 7 A low-magnification (x 15) SEM picture to see an overview of Sample C.

All the points revealed no Mg KLL, and furthermore no oxidized Mg LVV on C-3 contrary to the aforementioned two samples. Even on C-1 and C-2, I ratios of oxidized Al LVV to oxidized Mg LVV are much bigger to be 7.983 and 20.045, respectively. These facts are interpreted by the predominancy of Al oxide through the top 30 Å of the surfaces. On the other hand, the I_O KVV's are smaller than even Sample B indicating a less dense oxide.

AES depth-profiles of Sample B is shown in Fig. 8. Four characteristic zones are identified in the Figs. 8 and 9. First of all, a superficial contamination zone (Zone 1) up to an oxygen maximum, and Mg oxide-rich layer (Zone 2). This is followed by Zone 3, Al oxide-rich layer at the beginning and then a mixed state of oxide and metal, and finally substrate (Zone 4). The durations of sputtering for the first 3 zones are defined by τ_1, τ_2 and τ_3, respectively.

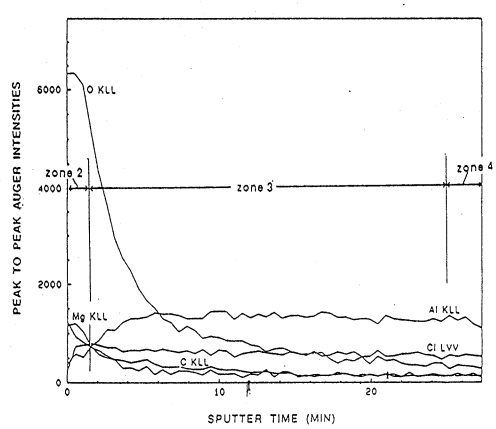

Fig. 8 AES depth-profile of Sample B.

Zone 1 is not seen for sample B, which is probably an effect of cleaning. τ_3 = 23.667 min >> τ_2, and the total sputter-time at $1/e\ I_O^{max} \equiv t_{oxide}$ = 4.0 min. This corresponds to a thickness ($\equiv z_{oxide}$) of ~ 80 Å. All the values turn out to be only 51 - 65% with respect to Sample A. This can be understood by the aforementioned fact that we had a more Mg oxide-rich layer at the top before depth profile than A. Fig. 9 is for Point C-1 showing quite different behavior. τ_1 was found again to be 1.5 min, but no Zone 2 seen in agreement with the analysis on its natural surface. τ_3 = 168.5 and t_{oxide} = 34.571 min (z_{oxide} ~ 691 Å), which are 7.1 and 8.6 times the corresponding values of Sample B, respectively.

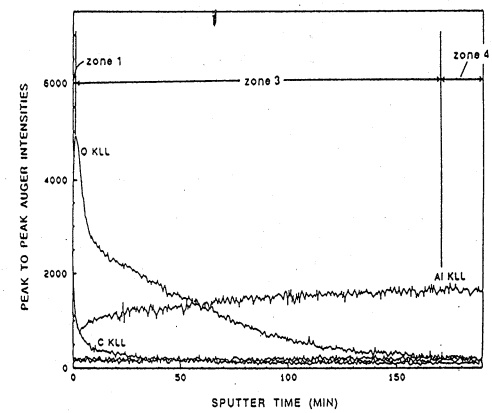

Fig. 9 AES depth-profile of Point C-1 on Sample C. Two nearly constant curves at a very low intensity are for Cl LVV and Mg KLL Auger peaks.

This relatively porous and thick oxide will provide a source itself of the synchrotron-induced desorption as well as a channel for outgassing from the bulk of chamber wall.

When the alloy material goes through extrusion, Mg can be segregated or evaporated remarkably through the initial thin Al-oxide layer[2] owing to high temperature (480 - 520°C) during process.[1,2] Therefore, Mg oxide is grown preferentially. Nevertheless, the amount of Mg is limited near surface immediately before and during the oxidation because its bulk composition is only 0.62 at.%. Consequently, the Mg-rich layer at the top should be thin,[2] and separated by a Mg-depletion layer from the ordinary bulk. Additional Al oxide-rich layer is grown beneath the initial Al oxide-rich layer. Nevertheless, the total thickness is smaller with the top Mg oxide-rich layer than that without it owing to the nature of Mg oxide-rich layer as a modifier.[3]

If the formed oxide layer at the top is broken away after extrusion, Al itself is exposed directly to chemical attack (especially during cleaning) and atmosphere. The grown Al oxide is less dense as already pointed out in terms of smaller I_O KVV's for every point on Sample C than even B, and accordingly thicker than the oxidation at extrusion. The cleaning procedure is thought to be the strongest interaction with the surface after extrusion. A small amount of strong acid like HCl can be dissolved from the cleaning solvent ($CH_3CCl_3 \rightarrow CH_2{=}CCl_2 + HCl$), especially under the conditions of bright light, heat, water mixed and catalytic metal mixed.[4] Then, it can etch out the superficial oxide at some places, particularly where the oxide layer has been shaken during high temperature and other preceding processes.

References

1. Y. Kato, K. Tsukamoto, E. Isoyama and T. Uchiyama, J. Vac. Soc. Jpn. **28** (11), 785 (1985).
2. B. Goldstein and J. Dresner, Surf. Sci. **71**, 15 (1978).
3. F. P. Fehlner, Low-Temperature Oxidation (Wiley-Interscience, New York, 1980) pp. 29, 116 -117.
4. S. Tsuji, ed., Fine Cleaning Technology Manual (New Technoogy Development Center, Japan) p. 27.